Engineering World
Open Access Journal
ISSN: 2692-5079

Thermal, Structural, Morphological and Dielectric Studies of Sol Gel Derived Codoped $SrTiO_{3-\delta}$

RAMANJEET KAUR and ANAND KUMAR TYAGI
Applied Science
I. K. Gujral Punjab Technical University
ramanjeetgill99@gmail.com
INDIA

Abstract: **- Gadolinium and Thulium doped $SrTiO_{3-\delta}$ i.e. $Sr_{1-x}Gd_xTi_{1-y}Tm_yO_{3-\delta}$ for $0\leq x\leq 0.30$ and $0\leq y\leq 0.05$ have been successfully synthesized using sol gel technique in this work. XRD patterns of the obtained ceramics are found to be sharp and well defined having no impurity phases for all the compositions. The lattice parameter 'a' decreases with amount of Gadolinium. Thermal Analysis, XRD, FESEM and EDX studies confirm the formation of $Sr_{1-x}Gd_xTi_{1-y}Tm_yO_{3-\delta}$ ($0\leq x\leq 0.30$, $0\leq y\leq 0.05$) ceramics with required cubic structure. FESEM/EDX analysis revealed that ceramics possess high density with marginal inter-granular porosity. The dielectric studies of the synthesized samples revealed that the synthesized samples possess high dielectric constants, high ac conductivity and low loss factors. The improvement in the dielectric properties of the synthesized samples has been observed with gadolinium and thulium doping.**

Key words: **Thermal, Structural, morphological, sol gel, codoped $SrTiO_{3-\delta}$, perovskite**

I. INTRODUCTION

Energy is the one of the basic requirements for sustainable development. The energy sources used nowadays suffer from many problems like global warming [1], various pollutions, their limited stocks etc. so renewable sources like wind, solar, hydrothermal energy etc were invented but these are dependent on climate conditions and are also less efficient

Fuel cell is one of the leading options available as efficient and environment friendly technologies that can generate power from renewable fuels like hydrogen etc. A fuel cell, like a battery, can generate electricity from electrochemical reaction. It can produce electricity as long as it is supplied the source of H_2 and O_2. Solid oxide fuel cells (SOFCs) are better than other fuel cell types like alkaline fuel cell, phosphoric acid fuel cell, molten carbonate fuel cell due to various limitations like requirement of pure fuel, expensive catalyst, corrosive electrolyte, high temperature requirement etc. [2-3].

Anode, cathode and electrolyte are the main components of SOFCs. The conventional materials i.e. nickel/copper – yttria stablized zirconia, rare earth doped ceria etc., used for the fabrication of different components of SOFCs, suffer from the various problems like sulfur poisoning, poor mechanical integrity, carbon deposition and lesser stability in reducing conditions. These problems put a major hurdle in commercializing this futuristic technology. The oxides with perovskite structure have emerged as good alternates as these can withstand the aforesaid problems. The most widely studied perovskites are Strontium titanates, Lanthanum chromites and their doped forms [4-9]. The doping of $SrTiO_{3-\delta}$ with various elements i.e. La, Ce, Sm, Gd, Dy, Y, Cu for Sr site and Fe, V, W, Mo, Ta, Nb for Ti site have been investigated by various research groups and enhancement in the ionic conductivity has been reported [10-11].

A number of synthesis routes have been employed to synthesize these perovskite materials in literature but all of them suffer from one or the other problems but sol gel based method offers a clean, contamination free and easy method for synthesizing these materials. In this study, Gd and Tm codoped $SrTiO_{3-\delta}$ i.e. $Sr_{1-x}Gd_xTi_{1-y}Tm_yO_{3-\delta}$ ($0\leq x\leq 0.30$, $0\leq y\leq 0.05$) have been synthesized using sol gel technique and investigated for thermal, structural, micro-structural and elemental composition using DTA/TGA, XRD and FESEM/EDS analysis.

ISSN: 2692-5079

II. EXPERIMENTAL WORK

A. Synthesis

$Sr_{1-x}Gd_xTi_{1-y}Tm_yO_{3-\delta}$ (x = 0, y = 0; x = 0.05, y = 0.005; x = 0.1, y = 0.005; x = 0.15, y = 0.02; x = 0.2, y = 0.02; x = 0.25, y = 0.05; x = 0.30, y = 0.05) samples had been synthesized via sol gel method employing titanium tetra isopropoxide $\{Ti(OC_3H_7)_4\}$, strontium acetate $\{Sr(CH_3COO)_2\}$, Gadlonium Nitrate $\{Gd(NO_3).6H_2O\}$ and thulium nitrate penta hydrate $\{Tm(NO_3).5H_2O\}$; all from Alfa Aesar™, as starting chemicals. The propanol, hydrochloric acid (HCl) and distilled water were used as solvents. In total seven samples had been prepared corresponding to various values of 'x' and 'y' i.e. x = 0, y = 0; x = 0.05, y = 0.005; x = 0.1, y = 0.005; x = 0.15, y = 0.02; x = 0.20, y = 0.02; x = 0.25, y = 0.05 and x = 0.30, y = 0.05 and were referred as STO0, STO1, STO2, STO3, STO4, STO5 and STO6 for respectively. The required amounts of raw chemicals were calculated using the metallurgical reaction (1).

$$(1-x)\ Sr(CH_3COO)_2 + x\ Gd(NO_3).6H_2O + (1-y)\ Ti(OC_3H_7)_4 + y\ Tm(NO_3).5H_2O \rightarrow Sr_{1-x}Gd_xTi_{1-y}Tm_yO_{3-\delta} \quad \ldots\ldots\ldots(1)$$

Firstly a 6wt% alcoholic solution of titanium dioxide (TiO_2) was prepared using titanium tetra isopropoxide (28wt%) as precursor, hydrochloric acid (13wt%) as catalyst, propanol (58wt%) and distilled water (1wt%) as solvent. A part of propanol was mixed with titanium tetra isopropoxide to form a solution (1) and the remaining amount of propanol, distilled water & HCl were mixed to form a solution (2). Both the solutions (1 & 2) were kept stirring at room temperature for 20 minutes and were then mixed to form the alcoholic solution. The alcoholic solution was stirred at room temperature for 24 hours and then calculated amounts of strontium acetate $\{Sr(CH_3COO)_2\}$, $Gd(NO_3).6H_2O$ and $Tm(NO_3).5H_2O$ were added to it to prepare the titania solution. The prepared solution was kept for 2-3 hours at room temperature, as a result of which the destabilized titania solution turned to homogeneous opalescent alcogel. The alcogel was then dried at ~ 80°C and crushed to obtain the fine powder [12]. The obtained powders were calcined at 600°C and then sintered at 1250°C for 2 hours at heating rate 3°C per minute.

The pellets of the sintered powders were prepared with the help of hydraulic press using PVA solution as binder. The binder was expelled by heating the pellets at 600°C for 1 hour at heating rate of 3°C per minute. The sintering was done before the pellet formation to avoid the pulverization of pellets. All the seven samples were prepared using the aforesaid technique in a single go.

B. Characterization

DTA/TGA/DTG analysis of uncalcined STO0 (x=0, y=0) and STO3 (x=0.15, y=0.02) powders was done under nitrogen atmosphere at heating rate 10^0C/minute using EXSTAR TG/DTA 6300 instrument. X ray diffraction analysis of the synthesized pellets was done with the help of XPERT-PRO X-RAY diffractometer 0000000011141934 using Cu K_α radiation. SEM/EDS analysis of the prepared pellets was carried out using using Nova Nano FE-SEM (FEI) for morphological and elemental analysis. The dielectric properties of the sintered the samples were studied with the help of LCR HiTester.

III. RESULTS AND DISCUSSION

A. Thermal Analysis

DTA/DTG/TG thermograms for uncalcined powders of STO0 (x=0, y =0) and STO3 (x=0.15, y=0.02) samples are shown in fig.1. Clearly, DTA/DTG/TG curves for both the samples; STO0 and STO3 are almost same. These can be divided mainly in three parts. First part of TG curves corresponds to heavy weight loss from 99% to 78% in the temperature range from 26°C to 239°C with two endothermic peaks at 69°C & 130^0C and 78°C & 146°C for STO0 and STO3 respectively. The weight loss and endothermic peaks are due to the evaporation of some remainders of solvents with rise in the temperature. Second part of TG curve corresponds to weight loss of 17% (STO0) and 22% (STO3) in the temperature range from 240°C to 815°C and exothermic peaks at 385°C and 476°C for STO0 (x=0, y=0) and STO3 (x=0.15, y=0.02) respectively. This is due to decomposition of the organic residues present within the samples with increase of the temperature. Third region corresponds to weight loss of approximately 9% in temperature range from 815°C to 1288°C with small endothermic peaks at 815°C and 827°C for STO0 and at 828°C and 874°C for STO3 sample. This region of the curves corresponds to the development of the required $SrTiO_{3-\delta}$ and $Sr_{1-x}Gd_xTi_{1-y}Tm_yO_{3-\delta}$ phase [12-15].

ISSN: 2692-5079

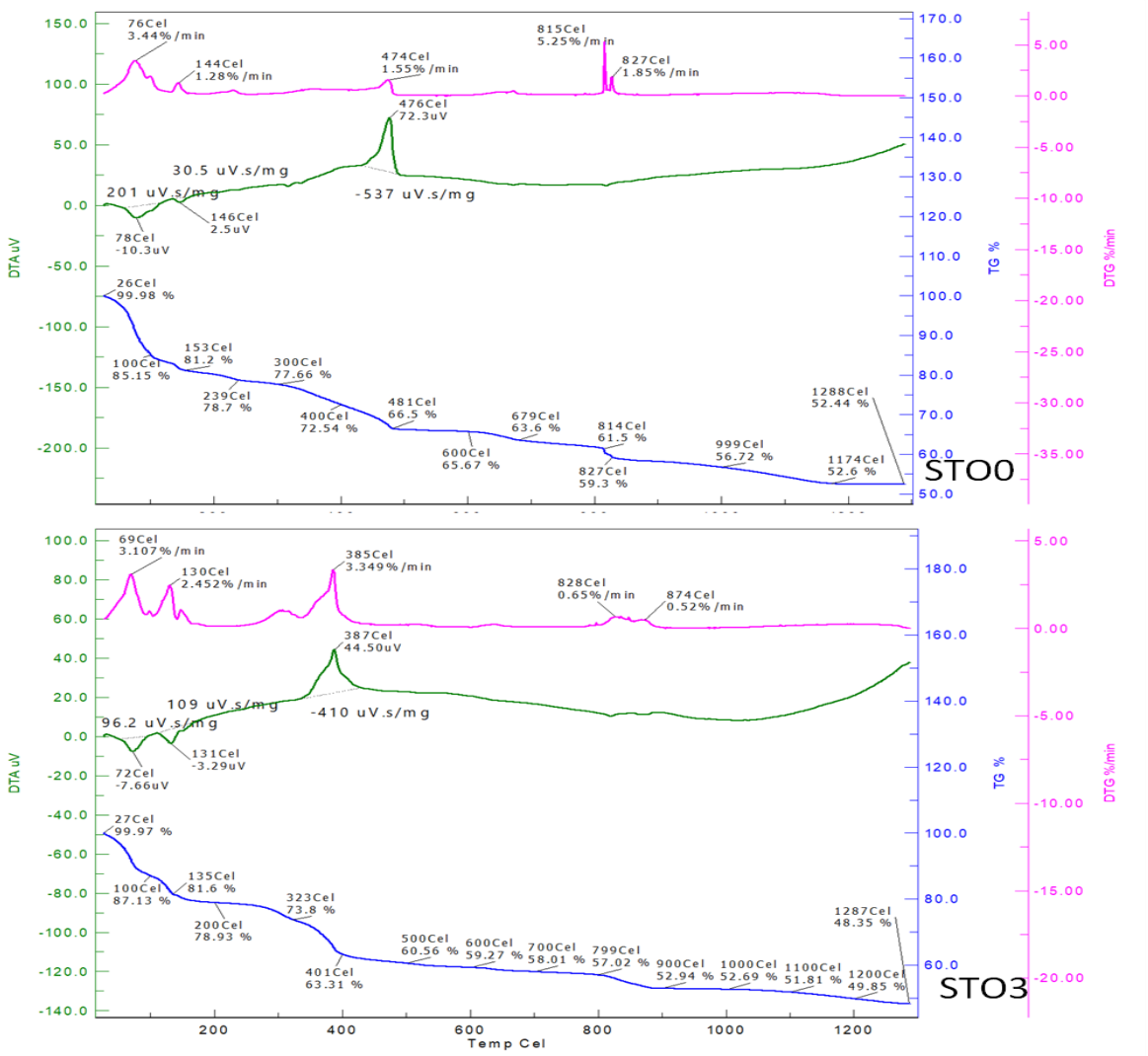

Fig. 1 DTA/DTG/TG curves for uncalcined powders of STO0 and STO3 samples

.

B. XRD Analysis

B.1 Phase development

XRD peak patterns of $Sr_{1-x}Gd_xTi_{1-y}Tm_yO_{3-\delta}$ samples ($0 \le x \le 0.30$, $0 \le y \le 0.05$) are shown in fig.2. Clearly, all the XRD peaks are well defined and are indexed on the basis of cubic symmetry of the structure using mathematical method [16]. The XRD patterns observed here are similar to the XRD pattern of $SrTiO_3$ reported in literature [12]. All the STO samples show nearly identical XRD patterns with no detectable impurity phases indicating the purity of the synthesized ceramics.

The shift of most intense peak (110) for $Sr_{1-x}Gd_xTi_{1-y}Tm_yO_{3-\delta}$; STO samples from pure sample i.e. STO0 with increase in gadolinium content and constant doping amount of thulium is shown in fig. 3. The peaks shift toward the larger angle side with increase in Gd content that may be attributed to intake of relatively smaller ion Gd^{3+}; ionic radius 107.8 pm, as a replacement of Sr^{2+} ions; ionic radius 132 pm, in the ceramic matrix. The replacement of the Sr^{2+} ion by smaller Gd^{3+} ion decreases the lattice parameter of the samples [10,17].

ISSN: 2692-5079

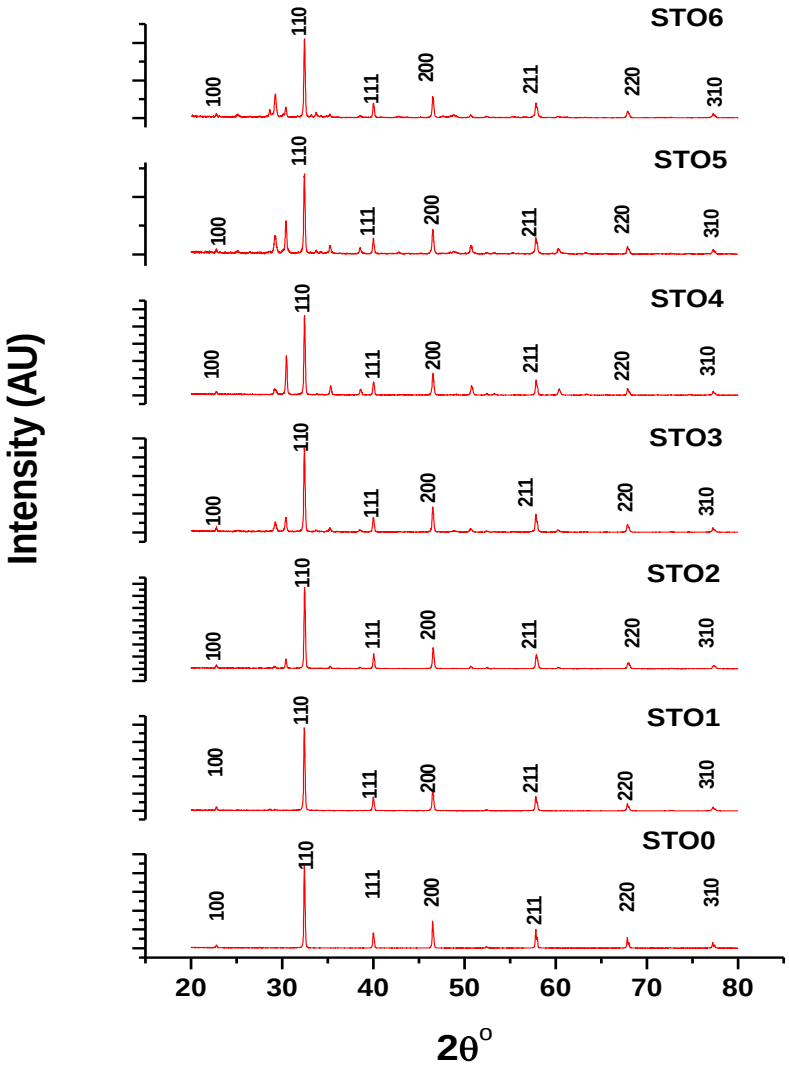

Fig. 2 XRD peak pattern for $Sr_{1-x}Gd_xTi_{1-y}Tm_yO_{3-\delta}$ samples ($0 \le x \le 0.30$, $0 \le y \le 0.05$)

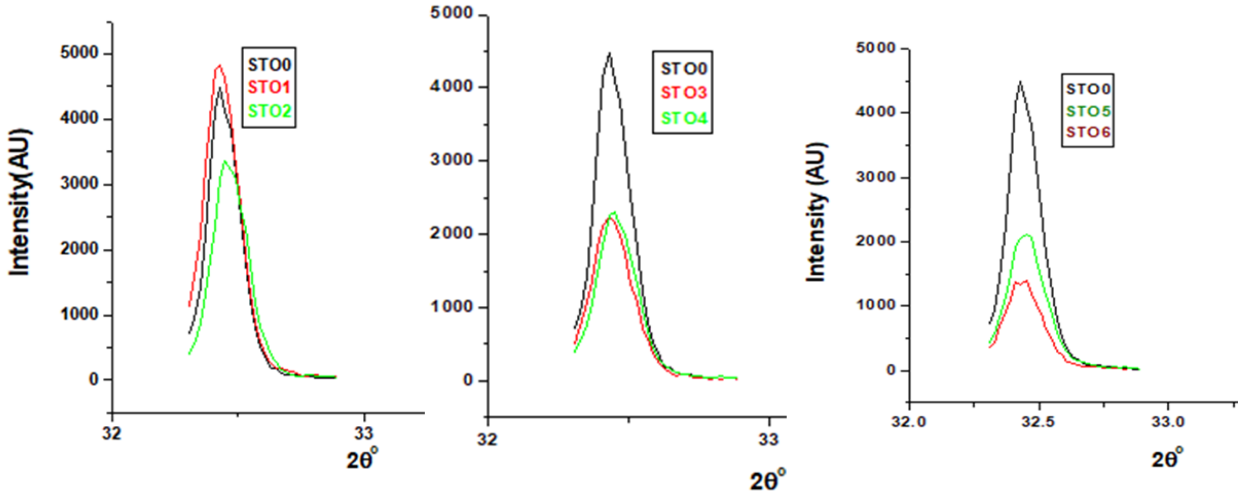

Fig. 3 Shift of the most intense peak (110) for $Sr_{1-x}Gd_xTi_{1-y}Tm_yO_{3-\delta}$ samples ($0 \le x \le 0.30$, $0 \le y \le 0.05$) with increase in 'Gd' content.

ISSN: 2692-5079

B.2 Lattice parameters

Table 1: Lattice parameter values for $Sr_{1-x}Gd_xTi_{1-y}Tm_yO_{3-\delta}$ samples ($0 \le x \le 0.30$, $0 \le y \le 0.05$)

Sample Code	x	y	Lattice Parameter (Å)
STO0	0	0	3.9114
STO1	0.05	0.005	3.9022
STO2	0.1	0.005	3.8984
STO3	0.15	0.02	3.9006
STO4	0.2	0.02	3.89975
STO5	0.25	0.05	3.90038
STO6	0.3	0.05	3.89983

The lattice parameters for the synthesized samples were calculated using mathematical method for cubic crystals[16]. The values of lattice parameter 'a' for all the doped $Sr_{1-x}Gd_xTi_{1-y}Tm_yO_{3-\delta}$ compounds are included in table 1. The variations of lattice parameter for $Sr_{1-x}Gd_xTi_{1-y}Tm_yO_{3-\delta}$ samples ($0 \le x \le 0.30$, $0 \le y \le 0.05$) for STO0, STO1 & STO2; STO0, STO3 &STO4 and STO0, STO5 & STO6 are shown in figures 4(a), (b) and (c) respectively. The figures 4, 5 & 6 clearly reveal that lattice parameter 'a' decreases from STO1 to STO2, STO3 to STO4 and STO5 to STO6; all values smaller than that for STO0; the pure undoped sample. The decrease in the lattice parameter is caused by replacement of Sr^{2+} (132pm) by the smaller rare-earth element Gd^{3+} (107.8pm) [17].

B.3 Crystallite Size

The crystallite sizes for all the synthesized samples were calculated for (110) reflection; the peak with maximum intensity, using the Sherrer's equation (2). The sherrer's equation [18] is:

$$d = \frac{k\lambda}{\beta \cos\theta} \quad \ldots\ldots(2)$$

Here d is crystallite size; k is constant, equal to 0.9, as the particles are assumed to be spherical, 'λ' is X-ray wavelength (1.5406 Å), β is FWHM and Θ represents the angle of diffraction for the peak under consideration. All the doped $Sr_{1-x}Gd_xTi_{1-y}Tm_yO_{3-\delta}$ samples have crystallite size lying in the range from 46 to 52 nm.

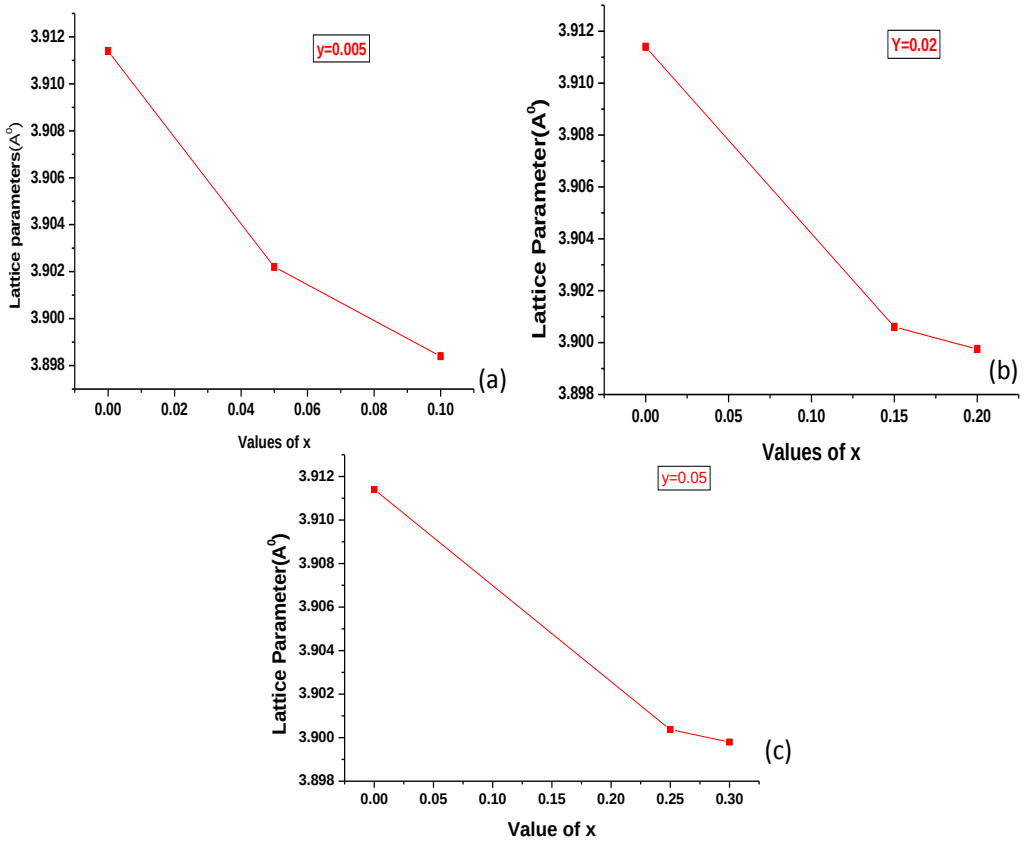

Fig. 4 Variation of lattice parameter 'a' with 'x' for (a) STO0, STO1 and STO2, (b) STO0, STO3 and STO4 with 'x' and (c) STO0, STO5 and STO6 with 'x'

ISSN: 2692-5079

C. FESEM Analysis

The microstructures of all $Sr_{1-x}Gd_xTi_{1-y}Tm_yO_{3-\delta}$; STO ($0\leq x\leq 0.30$, $0\leq y\leq 0.05$) samples as obtained by FESEM are shown in fig. 5. Clearly, all the samples are dense having homogeneous microstructure with well developed small angular grains. The grains have isotropic shapes close to spherical one for STO0 (x=0, y=0) to STO5 (x=0.25, y=0.05) ceramics; whereas the grain shape is cubiodal for STO6 (x=0.30, y=0.05) sample. The grain boundaries for all the prepared samples are smooth and clear having straight edges, well defined corners, faces without any extra phase precipitation. The straight edges confirm the high crystalline nature of the obtained ceramics, similar also revealed by XRD analysis. The synthesized STO samples have good sinterabiltiy and the low amount of inter-granular porosity as indicated by few residual and isolated voids present in the micrographs of STO samples. It is worth noting that the low heating rate used in the experiment i.e. 3ºC/min for sintering is favorable to the grain growth.

The microstructures of $Sr_{1-x}Gd_xTi_{1-y}Tm_yO_{3-\delta}$; STO samples have almost identical features, differing only in grain sizes. The grain sizes for $SrTiO_{3-\delta}$ samples as obtained from SEM analysis are in the range 407-972 nm, 83-587 nm, 104-750 nm, 234-747 nm, 169-426 nm, 179-618 nm and 43- 407 nm for STO0, STO1, STO2, STO3, STO4, STO5 and STO6 respectively; clearly in the nano range. The grain sizes of the synthesized samples are smaller than reported in the literature; that is normally in the micrometer range for the rare earth doped $SrTiO_3$ ceramics prepared by other techniques i.e. at high sintering temperature ~1300- 1470ºC [10, 19]. The nano size of the synthesized samples may be due to the fine precursor powders derived from sol-gel method and the low densification sintering temperature.

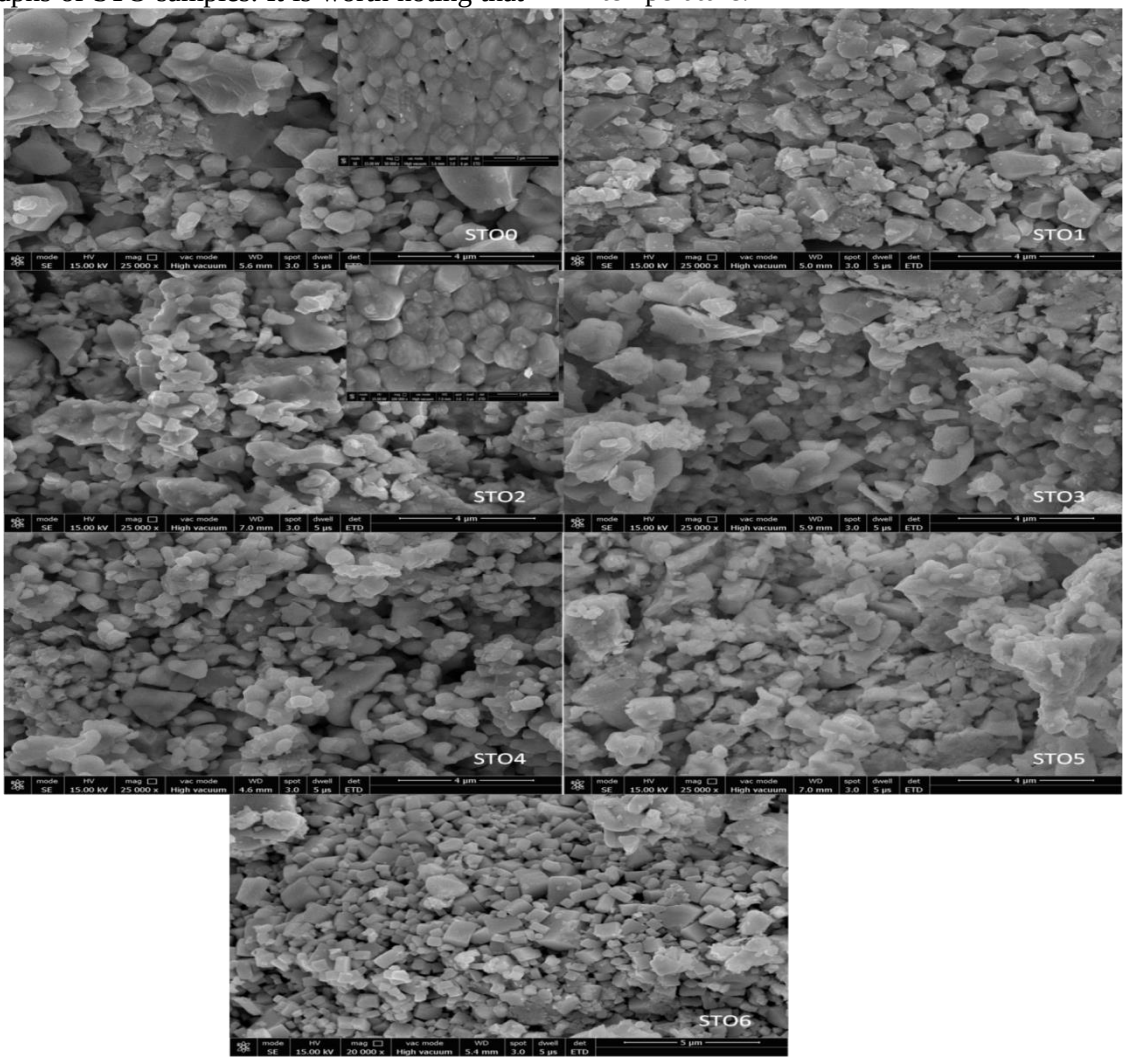

Fig. 5 FESEM image of $Sr_{1-x}Gd_xTi_{1-y}Tm_yO_{3-\delta}$ samples ($0\leq x\leq 0.30$, $0\leq y\leq 0.05$)

ISSN: 2692-5079

The grain growth in $SrTiO_{3-\delta}$ has been reported to be highly sensitive to doping amount [10, 20]. Here also, it can be easily realized that increase in Gadolinium and Thulium doping leads to gradual decrease of grain size; with minimum value of grain size for STO6. Thus, the high purity rare earth doped $SrTiO_{3-\delta}$ materials with high density have been successfully obtained by sol gel process at relatively lower sintering temperature.

D. EDX Analysis

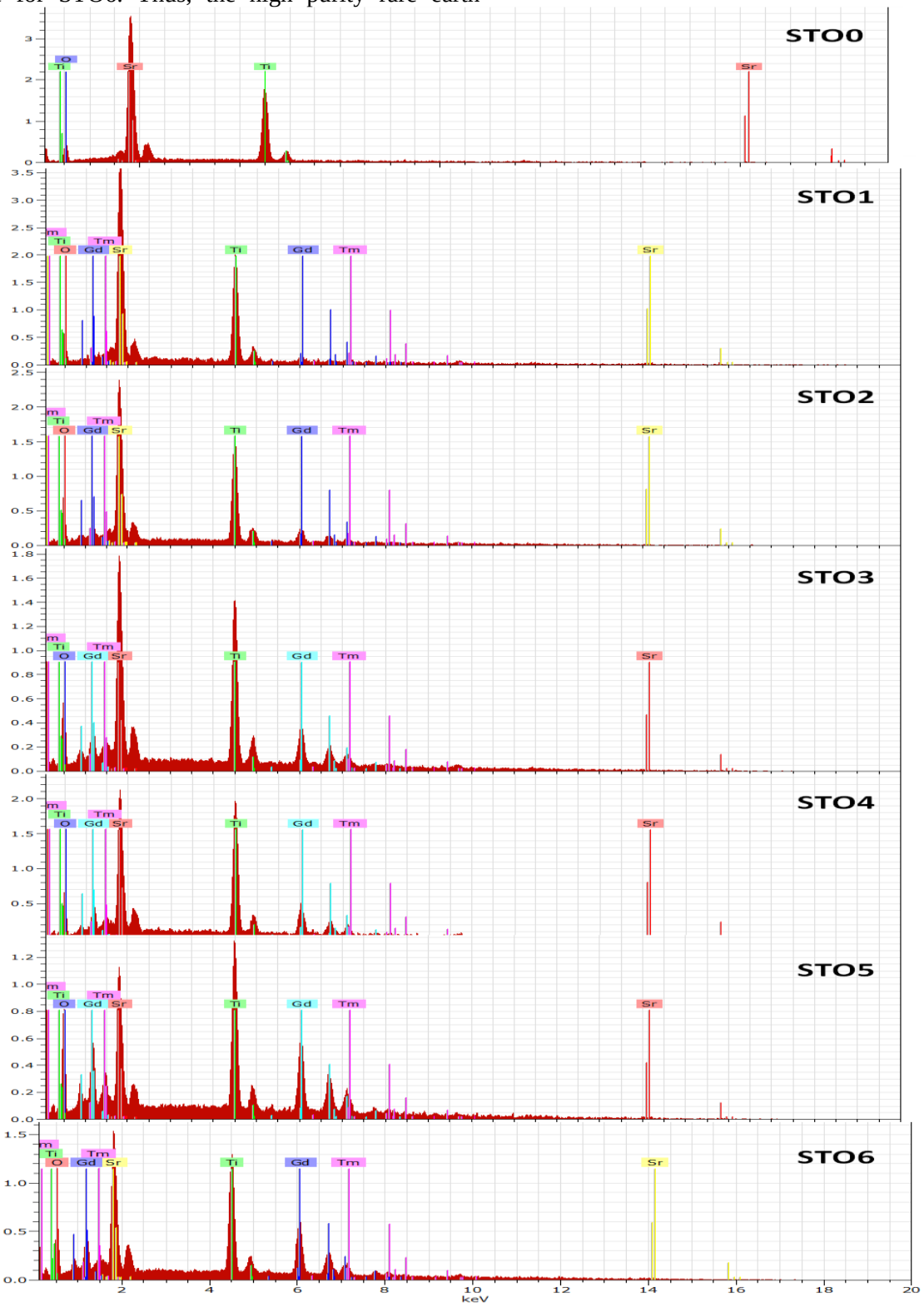

Fig.6 EDS spectra for $Sr_{1-x}Gd_xTi_{1-y}Tm_yO_{3-\delta}$ samples ($0 \le x \le 0.30$, $0 \le y \le 0.05$).

ISSN: 2692-5079

EDX spectra for $Sr_{1-x}Gd_xTi_{1-y}Tm_yO_{3-\delta}$ samples for all the compositions are shown in fig. 6. It can be easily observed from EDX spectra that only strontium, titanium and oxygen are present in STO0 (x=0, y=0), however, along with these elements, gadolinium and thulium are also present in the all other STO compositions. There is no evidence for any other element confirming the purity of the synthesized STO samples. Table 3 includes the atomic ratios of the elements for all the $Sr_{1-x}Gd_xTi_{1-y}Tm_yO_{3-\delta}$ samples ($0\le x\le 0.30$, $0\le y\le 0.05$) as obtained from EDS analysis, which are almost same as elemental ratio i.e. Sr + Gd : Ti + Tm : O = 1 : 1 : 3, calculated theoretically.

Table 3: Atomic ratio of elements for the $Sr_{1-x}Gd_xTi_{1-y}Tm_yO_{3-\delta}$ samples ($0\le x\le 0.30$, $0\le y\le 0.05$) from EDS analysis

Sample Code	x	y	Sr + Gd	Ti + Tm	O
STO0	0	0	1.26	1	3.29
STO1	0.05	0.005	0.6	1	1.94
STO2	0.10	0.005	0.64	1	2.6
STO3	0.15	0.02	1.03	1	3.08
STO4	0.20	0.02	1.22	1	2.89
STO5	0.25	0.05	0.88	1	2.29
STO6	0.30	0.05	1.04	1	3.25

The atomic composition of all the synthesized $Sr_{1-x}Gd_xTi_{1-y}Tm_yO_{3-\delta}$; STO samples as obtained from EDX analysis is given in the table 4. It is evident from the data included in the table that amount of gadolinium increases from STO0 to STO6 as expected and that of thulium also increases as required.

Table 4: Atomic composition of $Sr_{1-x}Gd_xTi_{1-y}Tm_yO_{3-\delta}$ samples ($0\le x\le 0.30$, $0\le y\le 0.05$) from EDX analysis

STO	Sr	Gd	Ti	Tm	O
STO0	1.26	0	1	0	3.29
STO1	0.55	0.07	1	0.07	2.08
STO2	0.54	0.14	1	0.06	2.8
STO3	0.92	0.19	1	0.08	3.33
STO4	0.74	0.21	1	0.09	2.51
STO5	0.74	0.41	1	0.11	3.61
STO6	0.93	0.48	1	0.16	3.34

3.5 Dielectric characterization

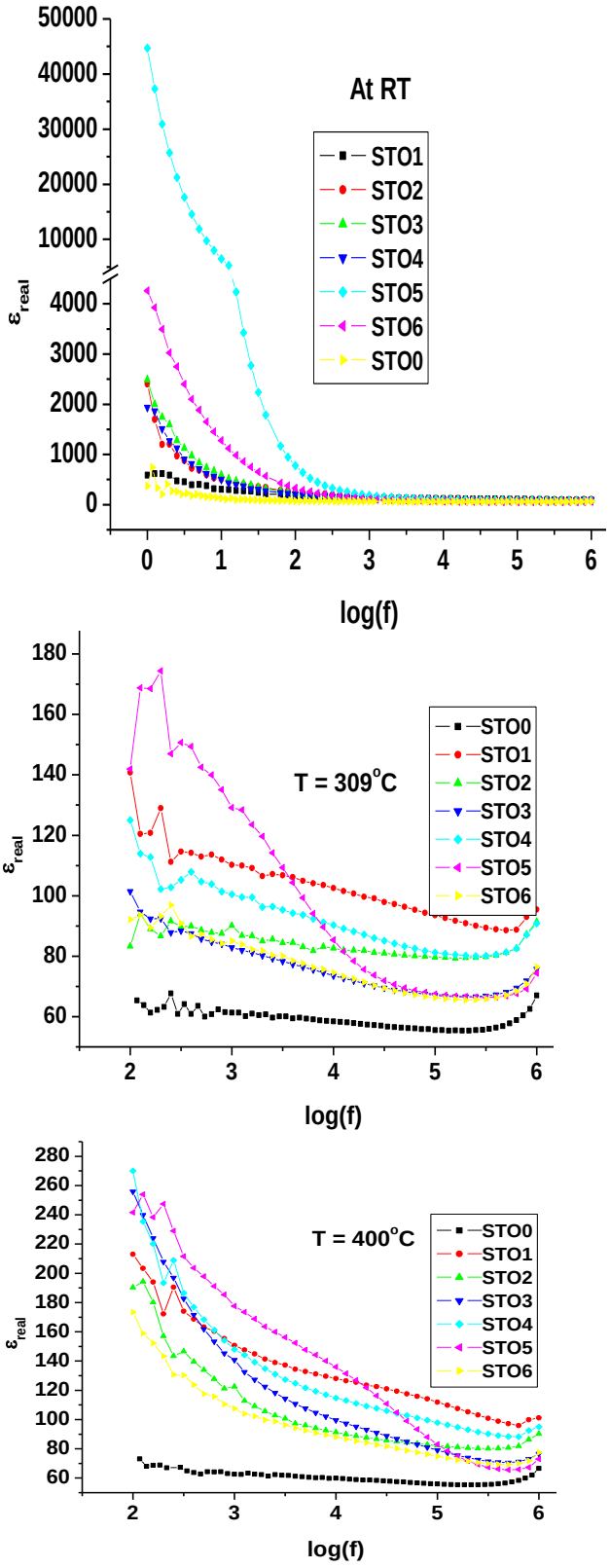

Fig. 7 Variation of dielectric constant with frequency at at room temperature, 309^{0}C & 400^{0}C for Gd, Tm doped $SrTiO_3$ samples

ISSN: 2692-5079

The values of dielectric constant (ε_r) were determined from the measured values of capacitance using the LCR meter between 30 - 400°C temperatures. The frequency dependence of ε_r at room temperature, 309^{0}C & 400^{0}C is shown in fig. 7 for all the doped samples. The variations of dielectric constant with temperature ranging from 50 to 400°C at frequencies 10 KHz, 100 KHz and 1 MHz for all STO compositions are shown in fig. 8. A sharp decrement in ε_r values with increase in frequency (<1 kHz) can be observed which may be due to the reason that at low frequency, contribution from electronic, ionic, orientation and space charge polarization exist but at high frequency only electronic polarization or some contribution from ionic polarization [21]. The strong dependence of dielectric constant on frequency up to 1 KHz is evident from fig. 8; which is termed as dielectric dispersion [22] and is quite common for dielectric materials. Whereas dielectric constant remains almost constant at frequencies above 1 KHz which is due to the reason that electric dipoles can't follow the fast varying electric field.

The dielectric constant remains almost constant up to a certain temperature and then, increases rapidly with increasing temperature (300–400°C). The space charge polarization arising from the movement of ions and defects in the material may be responsible for this increase [23]. There is no curie peak detected in the whole measurement temperature range [24-25]. The high values of dielectric constant at room temperature for all the STO samples may be attributed to the presence of all kinds of polarizations at room temperature which can lead to irregular increase in the permittivities [26-27]. It can be observed that doped STO compounds have larger dielectric constant values in comparison to undoped $SrTiO_3$; STO0 ceramic sample at all the studied temperatures and frequencies [28, 29].

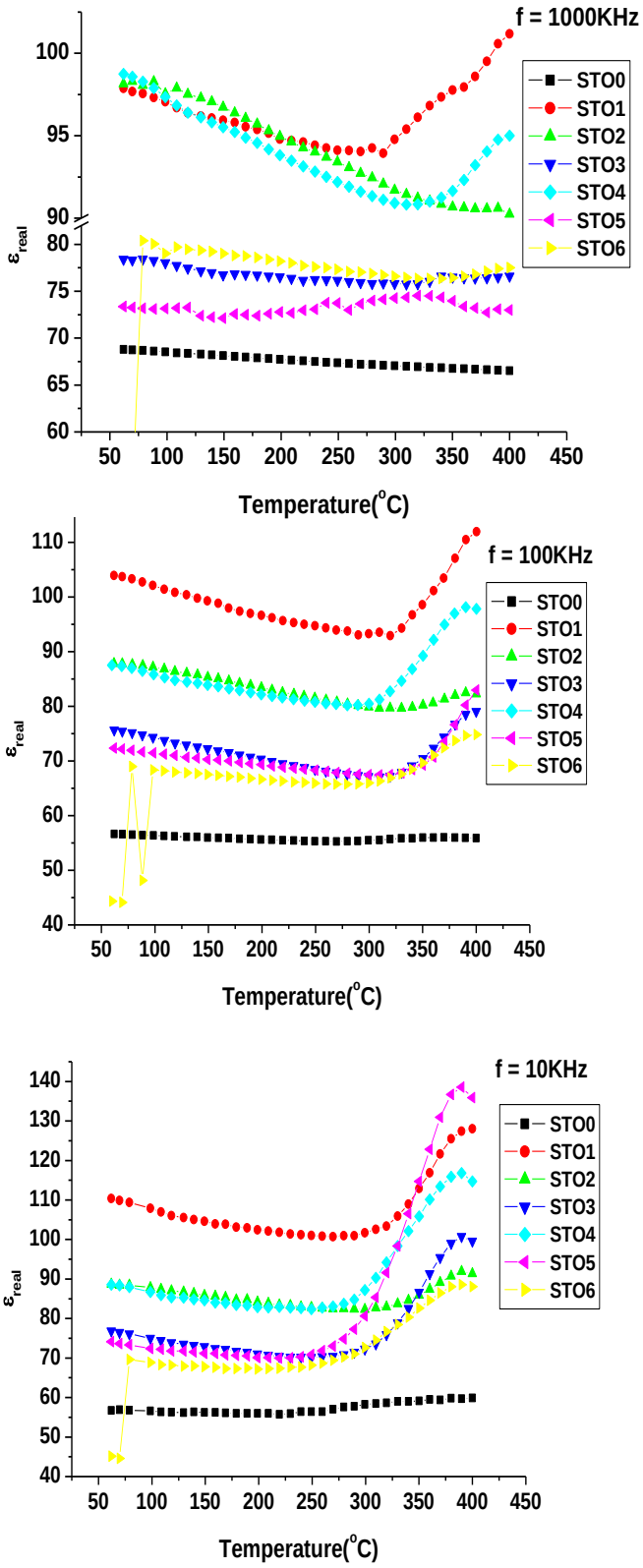

Fig. 8 Variation of dielectric constant with temperature at frequency 1000KHz, 100KHz and 10KHz.

ISSN: 2692-5079

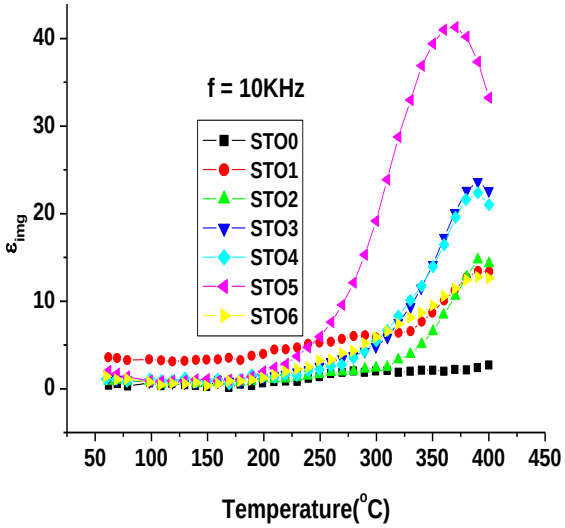

Fig. 9 Variation of imaginary part of dielectric constant with temperature at 10KHz for doped $SrTiO_3$ samples

Fig. 9 and 10 show the temperature and frequency dependence of imaginary dielectric constant (ε′′) for doped $SrTiO_3$ samples respectively. ε′′ shows the similar trends as that of ε_r i.e. increase with temperature and decrease with frequency. There is no loss peak in the whole frequency spectrum of ε′′. The values of ε′′ are high only at low frequencies (below 1KHz) and at high temperature (300°C to 400°C) owing to the interfacial build up of the free charges either within the sample (Maxwell-Wagner (MW) polarization) [30] or between sample and the electrodes (space-charge polarization). It can be easily observed that doping leads to increase in imaginary component of dielectric constant.

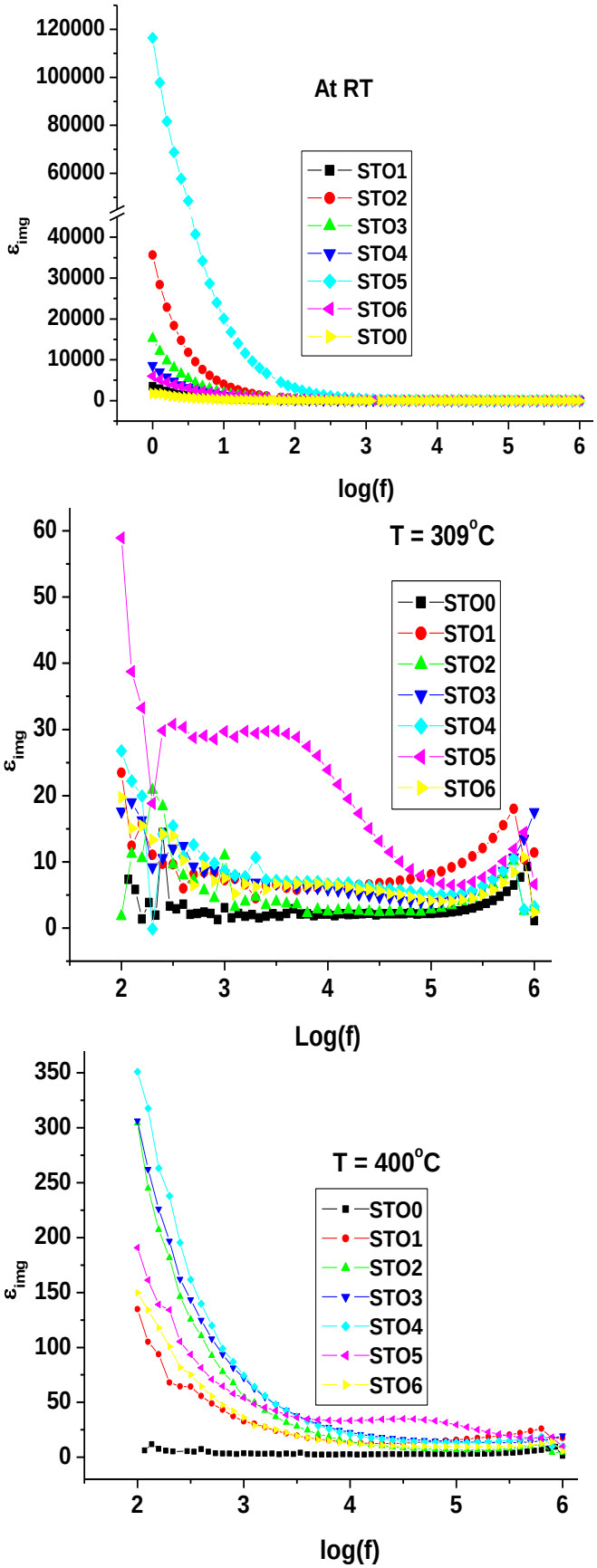

Fig. 10 Variation of imaginary part of dielectric constant with frequency at room temperature, 309°C & 400°C for doped $SrTiO_3$ samples

ISSN: 2692-5079

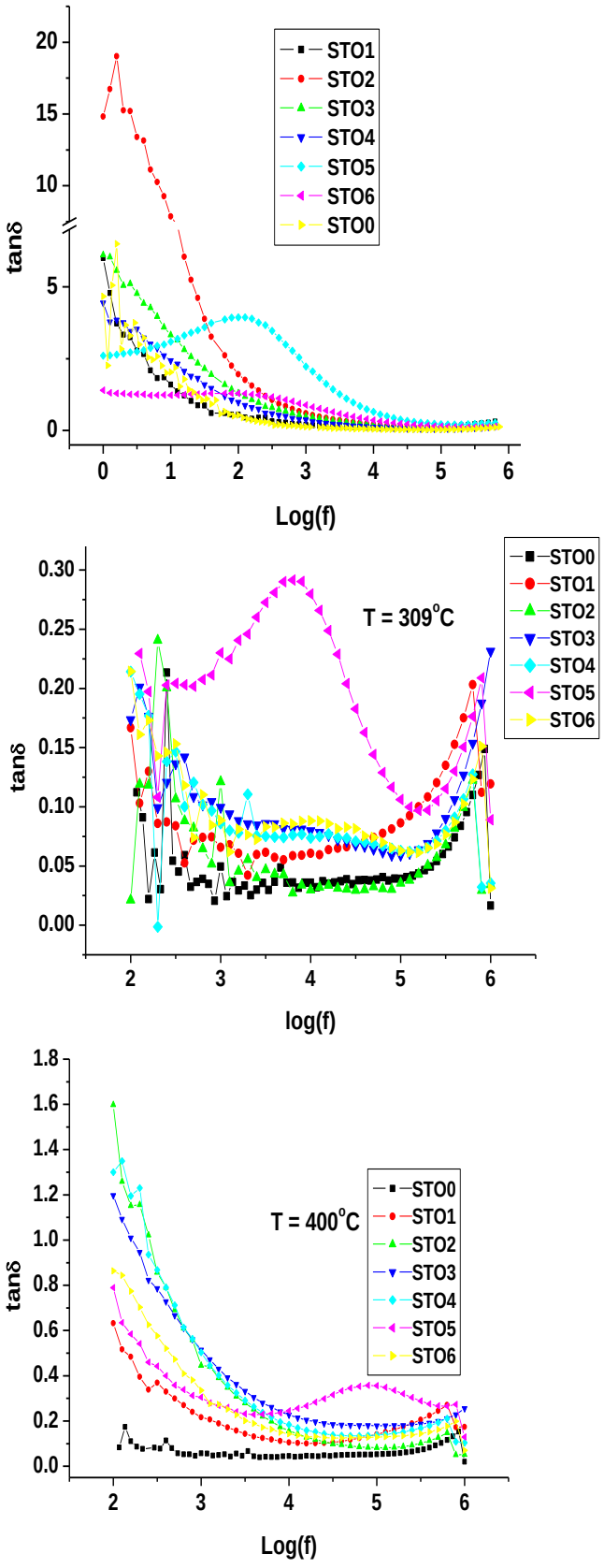

Fig. 11 Variation of dielectric loss with frequency at room temperature, 309°C and 400°C.

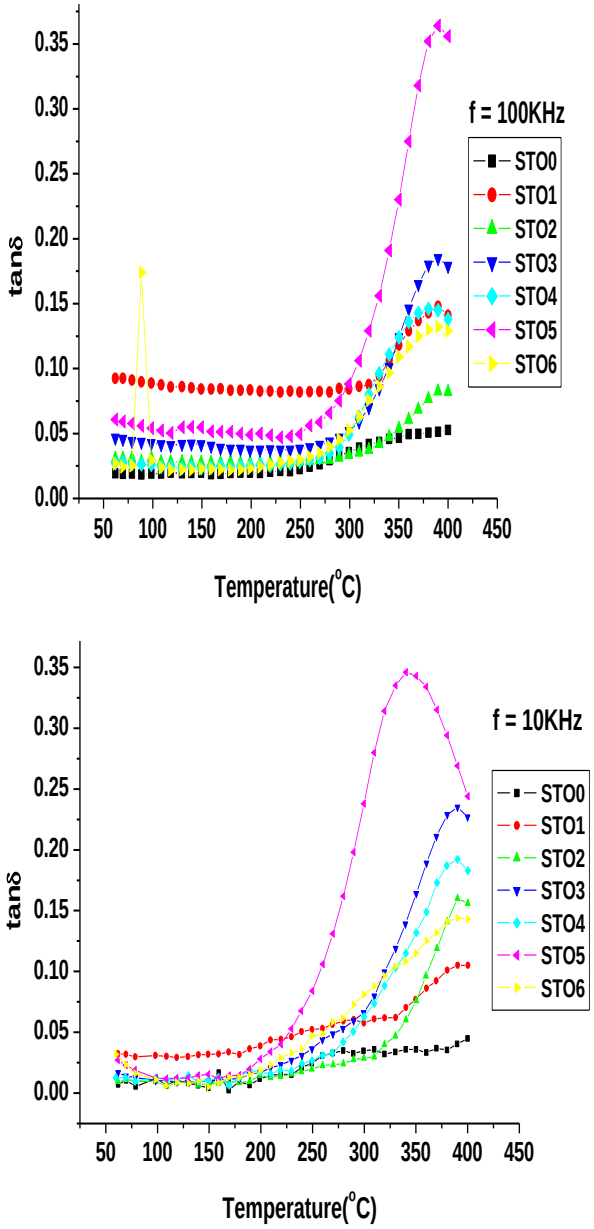

Fig. 12 Variation of dielectric loss with temperature at 100KHz and 10 KHz for doped $SrTiO_3$ samples

The variation of loss tangent for the doped samples with frequency at room temperature and at various temperatures i.e. 309, 400 is shown in fig. 11. Fig. 12 depicts the dependence of dielectric loss on temperature at frequencies 100 KHz and 10 KHz from 50 to 400°C. From all these plots, it can be easily observed that tanδ values decrease with frequency and increase with temperature. The decrease of dielectric loss with frequency can be explained using the relation [31]:

$\tan\delta \propto \sigma \backslash 2\Pi f$

where tanδ is the loss tangent factor, σ is the conductivity and f is the frequency. The increase in frequency is more than the increase in conductivity with frequency. So, loss tangent factor shows a

ISSN: 2692-5079

decrease with the increase in frequency within the entire temperature range.

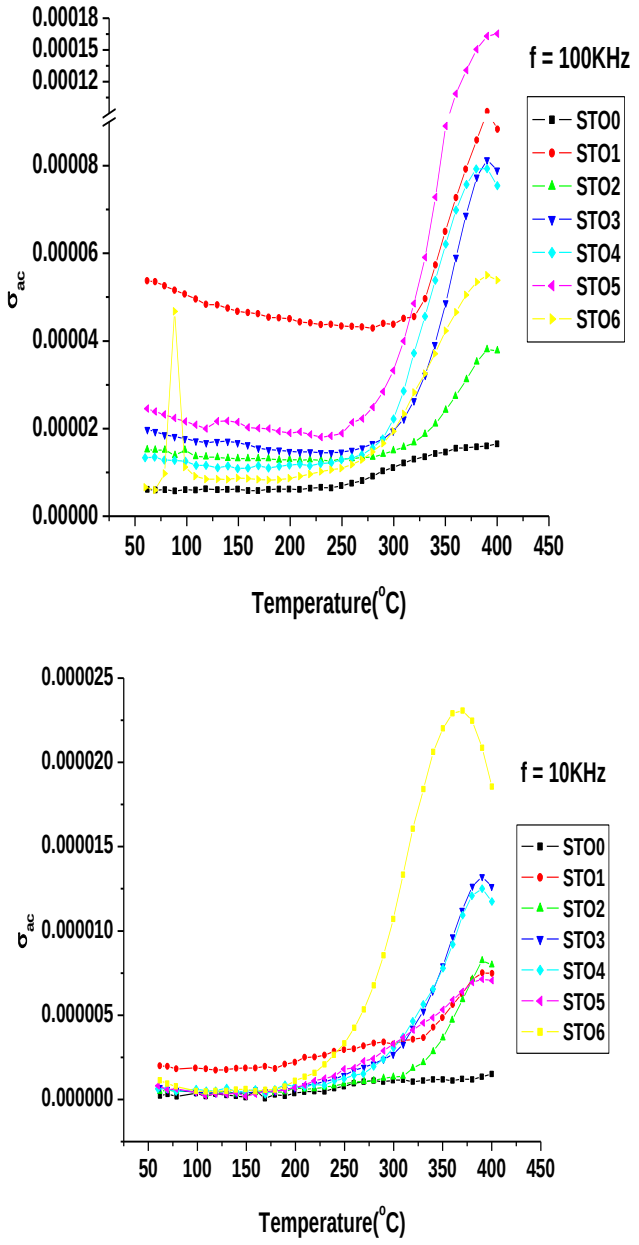

Fig. 13 Variation of ac conductivity with temperature at 100KHz and 10 KHz for doped $SrTiO_3$ samples

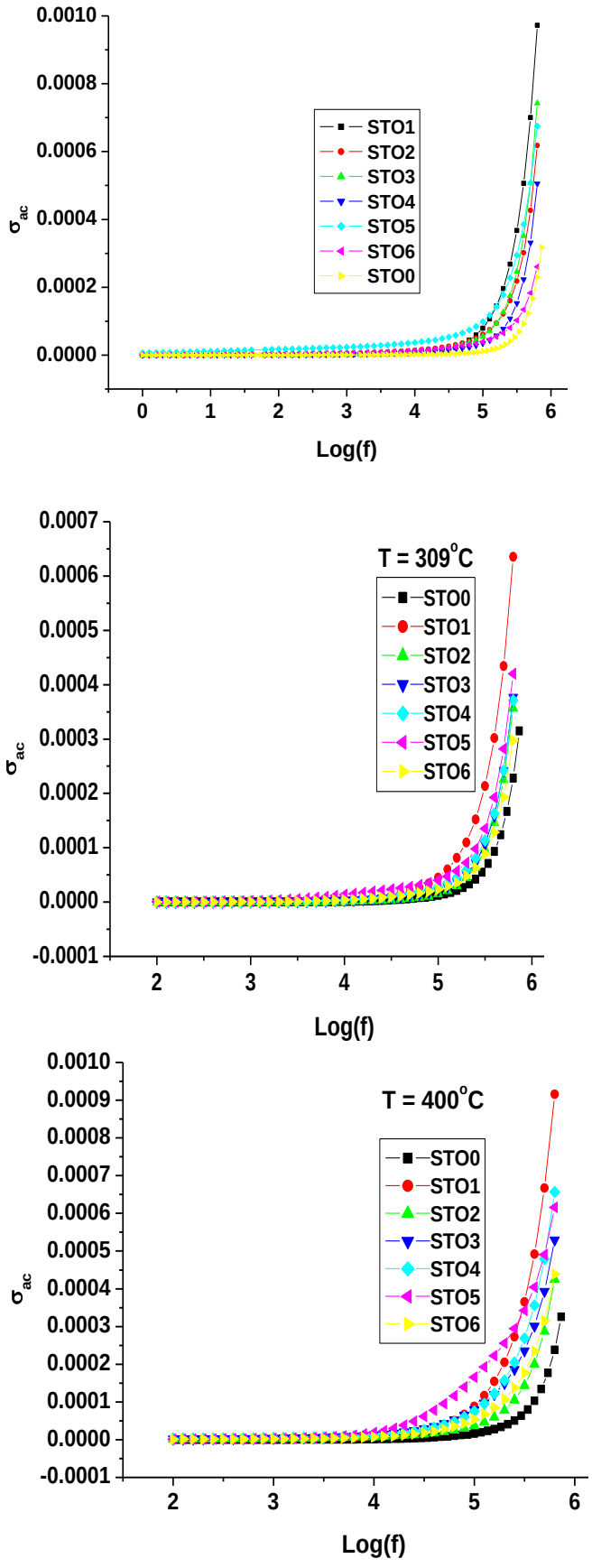

Fig. 14 Variation of ac conductivity with frequency at room temperature, 309°C & 400°C for doped $SrTiO_3$ samples

ISSN: 2692-5079

The observed enhancement in loss factor values at high temperature can be due to transportation of thermally energetic ions. The conductivity dominates at high temperatures due to presence of oxygen vacancies and defects created by oxygen loss at high temperature sintering; which leads to increase in loss factor also. In spite of this, the ferroelectric domain walls contribute less at high temperature leading to rise in loss tangent factor. Similar dielectric behavior has been reported in the literature for similar category compounds [24, 25, 27, 28].

The variation trends for the doped samples are approximately identical to that for undoped STO. The increase in loss factor with doping can be observed from above figures. In fig. 11, the dielectric relaxation for STO5 at ~ 10 KHz frequency can be observed which shifts to higher frequency with temperature rise [32].

Fig. 13 depicts the temperature dependence of ac conductivity at 10 KHz and 100 KHz frequency. The frequency dependence of ac conductivity at room and higher temperatures for all the doped STO samples is shown in fig. 14. It can be easily depicted that ac conductivity is almost constant at lower frequencies and at higher temperatures and frequencies there is a sharp enhancement in ac conductivity due to the strong hopping mechanism [33].

A plateau in the curves at low frequency and dispersion at high frequencies can be easily observed in the spectra. The conductivity which corresponds to the plateau region, is independent of frequency, and is termed as the DC conductivity. The transportation of the mobile ions due to applied field may be responsible for the observed plateau [34]. The observed trends for doped samples and pure STO0 sample are similar. It can be observed that doping with thulium and gadolinium gives rise to increase in ac conductivity in comparison to undoped STO0 samples. Similar trends were observed for yttrium [35, 36] or lanthanum [37, 38] doped strontium titanate, where conductivity showed an increase with increasing the doping amount [39].

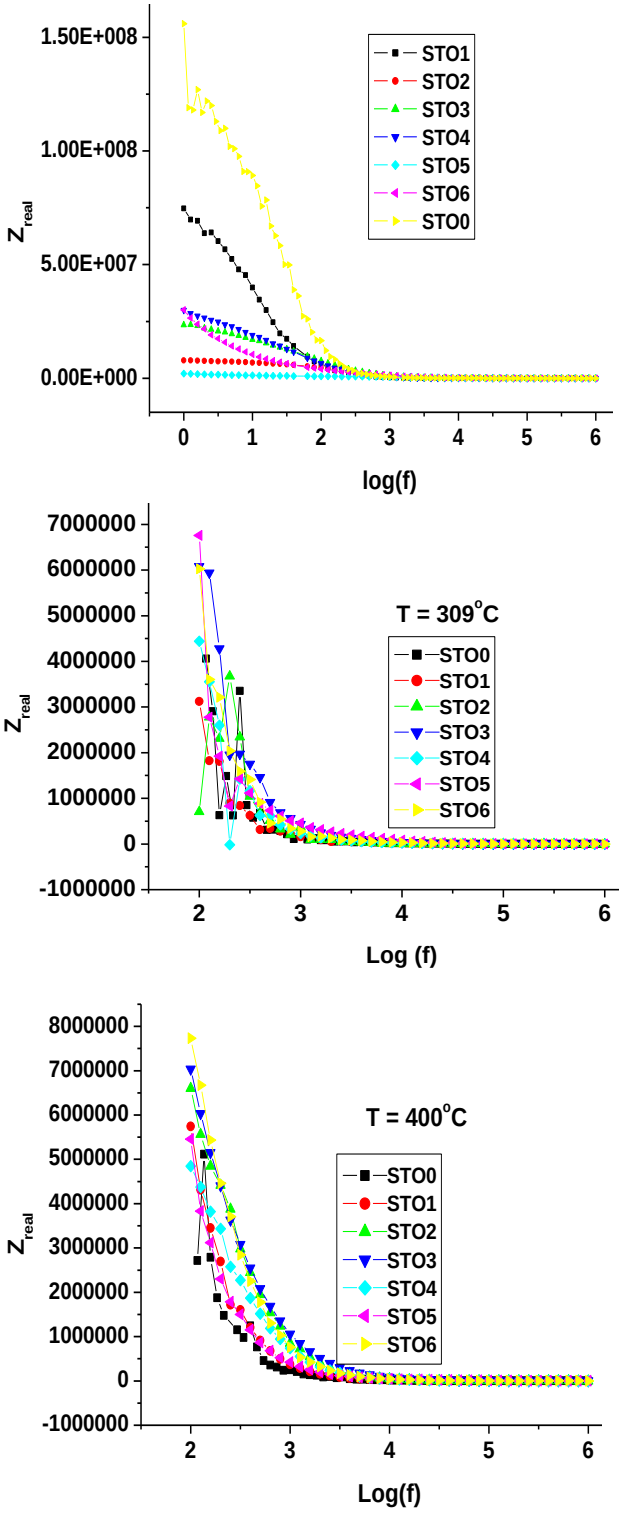

Fig. 15 Variation of real part of impedance with frequency at room temperature, 309^{0}C & 400^{0}C for doped $SrTiO_3$ samples

ISSN: 2692-5079

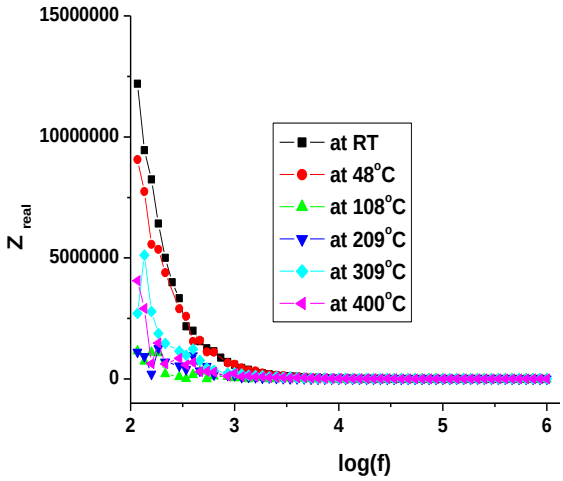

Fig. 16 Variation of real part of impedance with frequency at various temperatures for pure $SrTiO_3$ sample.

Fig. 15 shows the variation of the real part of impedance (Z') for all doped STO samples with frequency at room temperature, 309 and 400°C respectively and fig. 16 shows the variation of Z' with frequency for pure STO0 sample at various temperatures. The decrement in Z' with frequency as well as with temperature can be easily depicted from the two figures. The value of Z′ for all temperatures coincides at high frequency. All the doped samples show behavior similar to pure STO sample. The rise in temperature reduces the barrier which in turn leads to increase in ac conductivity and thus decrement in Z′. The decrease in Z′ with rise in temperature is very clear at low frequencies in fig. 16; revealing that synthesized materials possesses negative temperature coefficient of resistance.

Fig. 17 shows the frequency dependence of imaginary part of impedance (Z″) for all the doped samples at various temperatures. It can be easily depicted from the curves that Z″ values show a maximum value i.e. a peak in the plot; and this peak or maxima shifts towards high frequency value as the temperature is increased. The observed broadening of peaks in these plots may be attributed to spread of relaxation time i.e. the temperature dependence of electrical relaxation in the studied materials. Z″ values merge in the high frequency region, as clearly visible from the plots; this can be due to accumulation of space charges in the sample [34, 40-43].

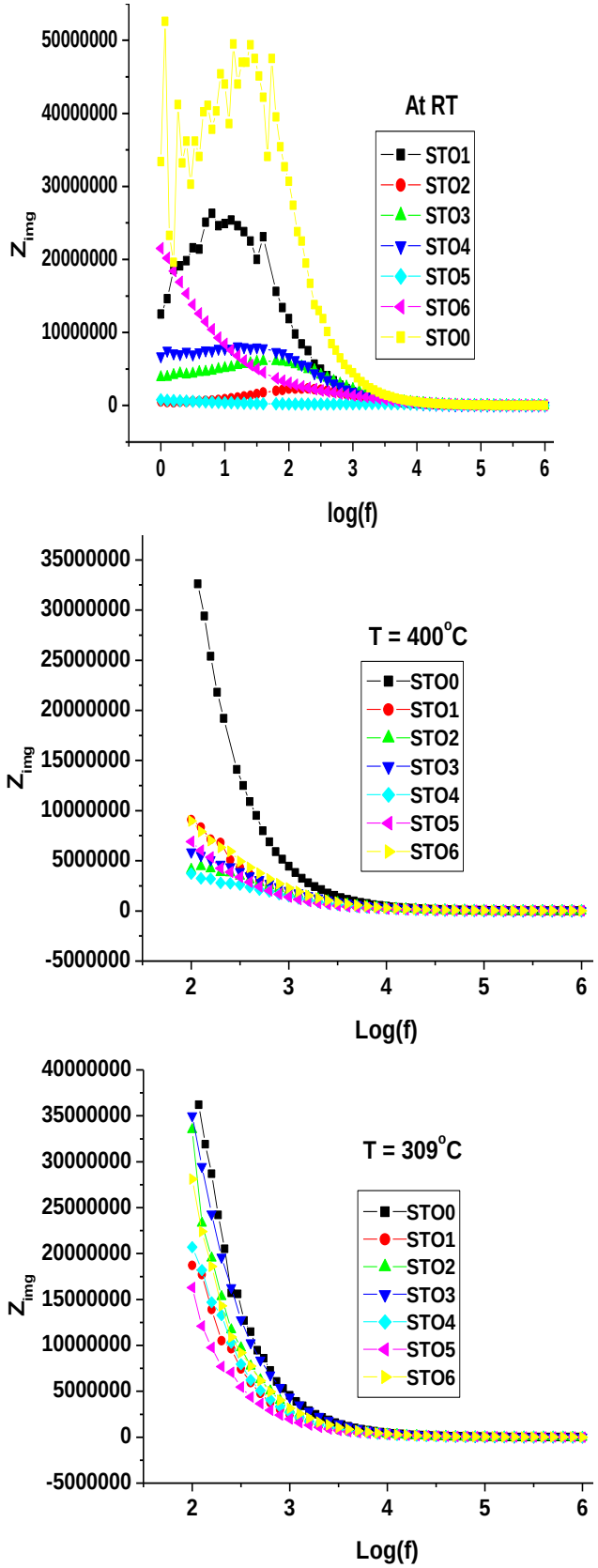

Fig. 17 Variation of imaginary part of impedance with frequency at room temperature, 309°C & 400°C for doped $SrTiO_3$ samples

ISSN: 2692-5079

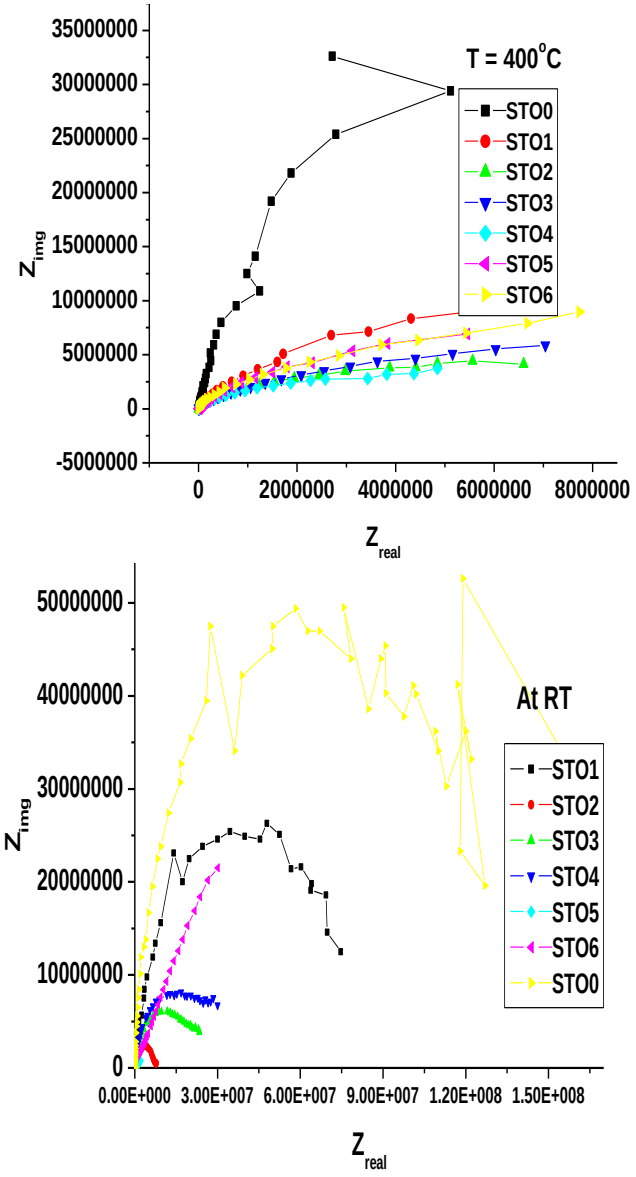

Fig. 18 Cole-Cole plots between real part (Z′)and imaginary part (Z′′) of impedance at room temperature and 400°C for doped $SrTiO_3$ samples

Cole-Cole plots can be used to explain the dielectric relaxation phenomenon within the studied frequency range. Fig. 18 shows the Cole-Cole plots (Nyquist plots) of doped STO ceramic samples at room temperature and 400 ℃. All the doped samples almost show the similar plots and radius of semicircle decreases with doping of gadolinium and thulium which shows that resistance decreases with doping. The presence of single depressed semicircle can be easily depicted from the plots for all the studied samples at room temperature as well as at 400°C; which represents the grain effect in the synthesized material. Furthermore, the increase in temperature leads to decrease in the semicircle radius indicating the decrement in the resistivity. The behavior of doped samples is similar to that of undoped STO sample [40].

IV. CONCLUSION

In this work, $Sr_{1-x}Gd_xTi_{1-y}Tm_yO_{3-\delta}$ ($0\le x\le 0.30$, $0\le y\le 0.05$) samples have been successfully synthesized using low temperature sol gel technique. The XRD patterns for all the compositions are sharp and well defined having no impurity phases. The lattice parameters decrease with increase in amount of Gadolinium. The microstructures of the synthesized STO samples are homogeneous, less porous and crystalline having nanometric grains. The doping with Gd and Tm further reduces the grain size. EDX analysis suggested that the ratio of strontium, titanium, thulium, gadolinium and oxygen is in close agreement with theoretical values. Thus, thermal, XRD and FESEM/EDX studies reveal the formation of phase pure $Sr_{1-x}Gd_xTi_{1-y}Tm_yO_{3-\delta}$ samples having cubic structure. All the synthesized STO samples possess high dielectric constants, high ac conductivity and low loss factors. The dielectric properties show enhancement with increase in content of gadolinium and thulium.

ACKNOWLEDGEMENT

One of the authors Ms. Ramanjeet Kaur highly acknowledges Inder Kumar Gujral Punjab Technical University, Kapurthala, for its valuable inputs in course of this work. The authors are also very thankful to TEQIP, MHRD/World Bank Project for facilitating the necessary research requirements. Furthermore, authors appreciatively acknowledge IIC, I.I.T. Roorkee, MRC, MNIT Jaipur and S B S State Technical Campus, Ferozepur for support in characterization of samples.

References

[1] National Oceanic and Atmospheric Administration, Climate of 2001, Annual review.
[2] Minh N. Q., *Journal of American Ceramic Society*, Vol.76, 1993, pp.563.
[3] Singhal S. C., *MRS Bulletin*, Vol.25, 2000, pp.16.
[4] Mukundan R., Brosha E. L. and Garzon F. H., *Electrochemical and Solid-State Letters*, Vol.7, 2004, pp.A5–A7.
[5] Cheng Z., Zha S. and Liu M., *Journal of Electrochemical Society*, Vol.153, 2006, pp. A1302– A1309.

[6] Cheng Z., Zha S. and Liu M., *Journal of Electrochemical Society*, Vol.153, 2006, pp. A1302-A1309.
[7] Morales J. C. R., Vázquez J. C., Savaniu C., Marrero López D., Zhou W. and Irvine J. T. S., *Nature*, Vol. 439, 2006, pp.568.
[8] Blennow P., Hansen K. K., Wallenberg L. R. and Mogensen M., *Solid State Ionics*, Vol.180, 2009, pp. 63–70.
[9] Radhakrishnan K., Tan C. L., Zheng H. Q. and Ng G. I., *Journal of Vaccum Science Technology*, Vol.1638, 2000, pp.A 18.
[10] Zhang L. , Tosho T., Okinaka N. and Akiyama T., Thermoelectric Properties of Combustion Synthesized and Spark Plasma Sintered $Sr_{1-x}R_xTiO_3$ (R = Y, La, Sm, Gd, Dy, 0 < x<0.1), *Materials Transactions*, Vol. 48, No. 8, 2007, pp. 2088-2093.
[11] Tolczyk M., Molin S., Gazda M. and Jasinski P., Structural and electrical properties of STF materials for SOFC applications, *Ceramic Materials*, Vol.63, No.1, 2011, pp.151-156.
[12] Rocca A., Licciulli A., Politi M. and Diso D. *International Scholarly Research Network Ceramics*, 2012.
[13] Donkelaar S. F. P., Ruhl R., Veldhuis S. A., Nijmeijer A. , Winnubst L. and Bouwmeester H. J. M., *Auto-combustion synthesis of perovskite-type oxides SrTi1-xFexO3-δ,* 8-9.
[14] Li B., Wang C., Liu W., Zhong Y. and An R., *Materials Letters*, Vol.75, 2012, pp.207–210.
[15] Ueno S., Nakashima K., Sakamoto Y. and Wada S., *Nanomaterials, Vol.* 5, 2015, pp.386-397.
[16] Laboratory Module, Indexing X-Ray Diffraction Patterns.
[17] Shannon R. D., *Acta Crystallographica*, Vol.A 32, 1976, pp.751–767.
[18] Cullity B. D., *Elements of X-Ray Diffraction*, (Addison-Wesley), 2nd edition, 1978.
[19] Wang H. C., Lei W. C., Su W. B., Liu J., Sun Y., Peng H., and Mei L. M., *Journal of American Ceramic Society*, Vol. 94, 2011, pp.838–842.
[20] Makarovaa M. V., Artemenkoa A., Kopecek J., Laufek F., Zemenovaa P., Trepakov V. A. and Dejnekaa A., *Scripta Materialia,*Vol.116, 2016, pp. 21–25.
[21] Verma A., Thakur O. P., Prakash C., Goel T. C. and Mendiratta R. G., Temperature dependence of electrical properties of nickel– zinc ferrites processed by the citrate precursor technique, Material Science and Engineering B, Vol.116, No.1, 2005.
[22] Badapanda T., Harichandan R.K., Mishra A., Anwar S., Relaxor ferroelectric behavior of $BaBi_4Ti_4O_{15}$ aurivillius ceramic, *Journal of Advanced Dielectrics*, Vol.3, No.2, 2013, pp.1350013.
[23] Abhijit P., Amitabha B., Structural, dielectric and electrical properties of lithium silicate ceramics: A comparative study, *Journal of Material Science: Materials in Electronics*, Vol.24, 2013, pp.1855–1862.
[24] Muhamad N. F., Osman R. A. M., Idris M. S., 3 and Yasin M. N.M., Physical and electrical properties of $SrTiO_3$ and $SrZrO_3$, *EPJ Web of Conferences*,Vol.162, 2017, pp.01052.
[25] Li W., Ma Z., Gao L. and Wang F., Preparation and Electrical Properties of $La_{0.9}Sr_{0.1}TiO_{3+\delta}$, *Materials*, Vol.8, 2015, pp.1176-1186.
[26] Wang X., Zhang B., Xu L., Wang X., Hu Y., Shen G. and Sun L., Dielectric properties of Y and Nb co-doped TiO2 ceramics, Scientific Reports, Vol.7, 2017, pp.8517.
[27] Ray A., Behera B., Basuy T., Vajandarz S., Satpathy S. K. and Nayak, Modification of structural and dielectric properties of polycrystalline Gd-doped BFO–PZO, *Journal of Advanced Dielectrics*, Vol.8, No.5, 2018, pp.1850031.
[28] Rout S. K., Panigrahi S. and Bera J., Characterization of Ni-doped $SrTiO_3$ ceramics using impedance spectroscopy, Indian Journal of Pure & Applied Physics Vol.42, 2004, pp. 741-744.
[29] Kumar S. A. and Naidu K. C. B., Structural and Dielectric Properties of Bi_2O_3 Doped $SrTiO_3$ Ceramics, *International Journal of ChemTech Research*, Vol.9, No.01, 2016, pp.58-63.
[30] Kumar S., Varma K. B. R., Relaxor behavior of $BaBi_4Ti_3Fe_{0.5}Nb_{0.5}O_{15}$ ceramics, *Solid State Communications*, Vol.147, 2008, pp.457–460.
[31] White M. A., Physical Properties of Materials; CRC Press: Boca Raton, FL, USA, 2011.
[32] B. Prijamboedi B., Takashima H., Wang R., Shoji A., and Itoh M., Large dielectric constant arising from space-charge polarization in a $SrTiO_3$ thin film grown on an $YBa_2Cu_3O_{7-\delta}$ layer, *Physics Status Solidi (a)*, Vol.202, No.14, 2005, pp.R152–R154.
[33] Naidu K. C. B., Sarmash T. S. and Subbarao T., Synthesis and Characterization of Mn doped $SrTiO_3$ ceramics, *International Journal of Engineering Research & Technology*, Vol. 3, No.1, 2014.
[34] Tanmaya Badapanda T., Harichandan R. K., Nayak S. S., Mishra A., Anwar S., Badapanda T., Frequency and temperature dependence behaviour of impedance, modulus and conductivity of $BaBi_4Ti_4O_{15}$ Aurivillius ceramic, *Processing and Application of Ceramics*, Vol.8, No.3, 2014, pp.145–153.

ISSN: 2692-5079

[35] Fu Q. X., Mi S. B., Wessel E. and Tietz F., *Journal of European Ceramic Society*, Vol.28, 2008, pp.811–820.
[36] Zhao H., Gao F., Li X., Zhang C., Zhao Z., *Solid State Ionics*, Vol.180, 2009, pp.193–197.
[37] Moos R., Härdtl K. H., Journal of Applied Physics Vol.80, 1996, pp.393–400.
[38] Li X., Zhao H., Gao F., Chen N., Xu N., *Electrochemistry Communications*, Vol.10, 2008, pp.1567–1570.
[39] Karczewski J., Riegel B., Gazda M., Jasinski P. and Kusz B., Electrical and structural properties of Nb-doped $SrTiO_3$ ceramics, *Journal of Electroceramics*, Vol. 24, 2010, pp.326–330.
[40] Sahoo S., Dash U., Parashar S. K. S. and All S. M., Frequency and temperature dependent electrical characteristics of $CaTiO_3$ nano-ceramic prepared by high-energy ball milling, *Journal of Advanced Ceramics*, Vol.2, No.3, 2013, pp.291–300.
[41] Murugan A. V., Navale S. C., Ravi V., Preparation of nanocrystalline ferroelectric $BaBi_4Ti_4O_{15}$ by Pechini method, *Materials Letters*, Vol.60, 2006, pp.1023–1025.
[42] Xie D. and Pan W., Study on $BaBi_4Ti_4O_{15}$ nanoscaled powders prepared by sol-gel method, *Materials Letters*, Vol.57, 2003, pp.2970–2974.
[43] Kennedy B. J., Kubota Y., Hunter B. A., Ismunandar and Kato K., Structural phase transition in the layered bismuth oxide $BaBi_4Ti_4O_{15}$, *Solid State Communications*, Vol.126, 2003, pp.653–658.